Effect of copolymer sequence on local viscoelastic properties in spherical coordinates around a nanoparticle

Mitchell F. Wendt,[†]

Advisors: Alex J. Trazkovich,[†,‡] and Lisa M. Hall[*,†]

†*William G. Lowrie Department of Chemical and Biomolecular Engineering, The Ohio State University, 140 W 19th Ave., Columbus, OH 43210*

‡*SEA Limited, 7001 Buffalo Parkway, Columbus, OH 43229*

E-mail: wendt.54@osu.edu,trazkovich.1@osu.edu,hall.1004@osu.edu

Abstract

A polymer nanocomposite consisting of a spherical nanoparticle surrounded by coarse-grained polymer chains is simulated. Two monomer types make up the polymers, differing only in their interactions with the nanoparticle. All atomic stress fluctuations are measured, converted to spherical coordinates centered around the nanoparticle, and used to estimate the local stress autocorrelation as a function of distance from the nanoparticle. The local stress autocorrelation is substituted into the relationship between the bulk stress autocorrelation and bulk dynamic modulus, analyzed in both radial shear and tangential shear geometries. The result is then treated as an estimate of the local dynamic modulus. This allows us to separate radial and tangential effects on overall dynamic modulus as a function of distance from the nanoparticle for multiple copolymer sequences. Unlike the direction-independent results, short block length copolymer sequences exhibit a non-monotonic progression of the magnitude of the $tan(\delta)$ (hysteresis) peak over distance to the nanoparticle, suggesting that adjusting copolymer sequence could significantly control observed nanocomposite dynamics.

Introduction

Note: Some text and figures are adapted and reprinted with permission from A.J. Trazkovich.; M.F.Wendt.; L.M. Hall. Macromolecules, 2019. doi:10.1021/acs.macromol.8b02136.130.

Polymer nanocomposite materials are widely used in commercial applications such as tire rubber, bio-hybrid nanofibers, and other industrial, commercial, and scientific applications. Previous research efforts have analyzed the connection between polymers, nanoparticles, and composite properties, including dynamic properties such as modulus and energy dissipation, in order to improve the design of composite materials.[1–12] Specifically, these efforts have sought to use molecular dynamics simulations to study these materials, and particular attention has been devoted to explaining the difference in dynamics and rheology near the surface of nanoparticles compared to in the bulk. Due to the high surface-to-volume ratio of nanoparticles, local effects on material properties in the polymer-nanoparticle interphase have an exaggerated effect on the overall behavior of the composite material. It has been made clear that local dynamics in the polymer-nanoparticle interphase are different than in the bulk polymer, which is one reason why adding nanoparticles has such a large effect on the composite properties.[13–23] Through analysis of local dynamics and rheology at the nanoparticle surface, it is possible to achieve a better understanding of how to control polymer nanocomposite behavior.

Dynamic properties in the polymer-nanoparticle interphase are significantly influenced by the polymer-nanoparticle interaction strength. In the majority of industrial and commercial applications, favorable polymer-filler interactions are desireable becuase they can prevent nanoparticle aggregations that would otherwise occur. Polymers with a stronger interaction strength adsorb on the surface of nanoparticle, resulting in slower dynamics in the polymer-nanoparticle interphase.[24–29] When components are selected in applications such that polymer-nanoparticle interactions are unfavorable, interphase dynamics may be

faster than the bulk. Polymer-filler interaction strength is dependent on the monomer types and nanoparticle surface chemistry, so interphase properties can be adjusted by functionalizing the nanoparticle surface or changing the polymer chemistry.

Nanoparticle loading, a system variable easy to adjust in commercial applications, directly correlates with the extent that interphase properties impact the overall material behavior. As more nanoparticles are introduced into the system, the overall composite properties usually begin to more closely resemble those of the interphase (up to a certain threshold, above which filler-filler network effects become more significant).[30,31] Relationships between interphase properties, nanoparticle volume fraction, and the overall composite properties have been characterized in previous works.[32–35] Therefore, it is beneficial to understand interphase properties in rational material design.

One material property material designers frequently consider is elastic modulus, which measures a material's stiffness and resistance to deformation under static load. Typically, adding nanoparticles with strong interactions with polymer chains increases elastic modulus.[32,36] Experimental studies have measured local static elastic modulus to prove that modulus increases in the interphase between polymer and hard surfaces, provided that the polymer has a strong attraction to the surface.[37–39] Local static elastic modulus can also be measured in simulations, where a sum of local atomic forces can be used to calculate the theoretical instantaneous elastic modulus that would be experienced in response to a uniform, infinitesimal strain.[40,41]

Although previous studies have measured local static modulus, few previous works have considered local dynamic modulus. Dynamic modulus, which varies as a function of the frequency of applied strain, can be described as the sum of a storage modulus and a loss modulus, which respectively are the components of the response in phase and out of phase with the applied oscillatory strain. The ratio of the loss modulus to the storage modulus gives the ratio of the amount of energy lost to the amount of energy returned in a single strain cycle, and it is therefore a measure of the material's viscoelastic hysteresis.

While a previous study has been able to analyze dynamic moduli and hysteresis under Cartesian coordinates, this study is not able to separate radial and angular effects on these parameters due to the nanoparticle.[42] In the current work, we measure local dynamic moduli using a similar method, but we extend the analysis by considering the results in spherical coordinates, allowing us to examine the modulus in response to radial and tangential stress separately. Separately analyzing radial and angular dynamic moduli provide for a broader understanding that explains observed dynamic behaviors, providing clarity as to what the driving forces are behind the local behavior.

Dynamic moduli and hysteresis are important in applications where cyclic or changing loads are regularly applied to a polymer nanocomposite material. While low hysteresis is desirable in reducing energy loss and heat build-up within filled rubbers, high hysteresis is desirable in dissipating energy under cyclic load. Some applications may require low hysteresis under one set of operating conditions while maintaining high hysteresis under a different set of operating conditions, which poses even greater design challenges for material designers. For instance, in tire applications, maintaining low rolling resistance (which is desireable for good fuel economy) requires low hysteresis at lower loading frequencies correlated to rotation of the tire,[43–45] while achieving good traction requires high hysteresis at higher loading frequencies correlated to tread surface deformations while sliding across asperities on a road surface.[46,47]

In the current work, nanoparticles are incorporated into copolymer systems with two monomer types in various sequences. Several previous simulation studies have considered nanocomposites with adjustable copolymer sequences, with the majority of these examining effects of copolymer chain sequence on nanoparticle interactions.[48–50] When multiple polymer components interact at the nanoparticle surface, the resulting dynamics include interesting and sometimes surprising effects. For example, a significant body of work from the Akcora group has studied nanoparticles coated in highly adsorbing chains of a homopolymer with relatively high glass transition temperature (T_g) that are dispersed in a

matrix of a different homopolymer with a lower T_g.[51–53] It is well-known that, in blocky copolymer systems, unfavorable interactions between different monomers may cause microphase separation, which may in turn affect the polymer-nanoparticle interphase, the composite modulus,[54,55] and nanoparticle dispersion.[56–60] Previous simulation studies have specifically examined polymer-nanoparticle interphase properties and have determined that chain conformations around a nanoparticle depend on both the interaction strength of the two monomer types[61] and the copolymer sequence.[62] Other previous simulation work has shown that even when monomer-monomer interactions are all equal and monomers differ only in their interactions with nanoparticles (which is the case in this current work), chain conformations near nanoparticles still depend on copolymer sequence.[63–66] Considering such an idealized system allows us to focus on the effect of adsorption strength without confounding effects of any microphase separation in the bulk.

This work uses the same model as in our previous simulation study on dynamic moduli and hysteresis,[42] a simple nanocomposite consisting of a single spherical nanoparticle incorporated in a copolymer melt. Two monomer types are used, differing only in their strength of adsorption to a nanoparticle, and the blockiness of the copolymer sequence is adjustable (Figure 1). As found in our prior work, copolymer sequence affects the distribution of monomers in the interphase, the polymer radius of gyration, and the end-to-end autocorrelation, bond vector autocorrelation, and self-intermediate scattering function relaxation times, all of which tended to increase with proximity to the nanoparticle and with copolymer block length.[67] Using the same method to analyze atomic stress fluctuations and estimate the dynamic mechanical properties in the interphase as our previous study,[42] the dynamic moduli and hysteresis are now converted into spherical coordinates with respect to the nanoparticle, with radial and angular shear moduli and hysteresis being separately analyzed. This method is used to show that copolymer sequence has a significant effect on interphase material properties, and that these effects vary depending on the direction of which oscillatory strains are applied to the polymer-nanocomposite material. Although

the ability to obtain a true measurement of local dynamic modulus is hindered by the fact that particles move during the simulation time window associated with a given strain frequency, our results still describe the effects of copolymer sequence on the local properties in the polymer-nanoparticle interphase.

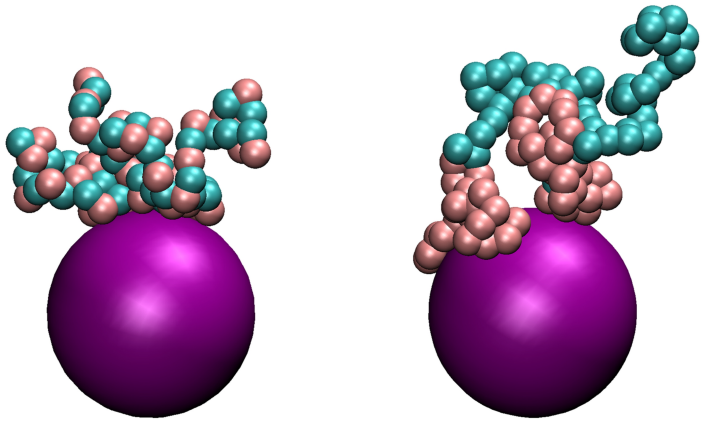

Figure 1: Snapshots of selected polymers from two simulated polymer-nanocomposite systems. Pink beads adsorb more strongly to the nanoparticle (purple) than cyan beads. The system on the left has a shorter block length than the system on the right, and subsequently has less microphase separation at the surface of the nanorparticle.

Methods

Before discussing the methodology used in this work, it is noteworthy to mention that no new simulations were conducted for this study, as all necessary simulations were conducted in our previous work.[42] The significant differentiation from the previous work is that the analysis of local dynamic moduli is now conducted in spherical coordinates centered at the nanoparticle center. Therefore, the simulation methods are identical to those used in the previous paper. The simulation methdods used previously, as well as methods of conversion to spherical coordinates are outlined in this section.

This work uses a standard attractive Kremer-Grest bead-spring model[68,69] where polymers are freely-jointed chains of coarse-grained monomer beads. Each of our systems consist of 400 linear chains of length $N = 100$ (which are analytically predicted to have

fewer than two entanglements per chain[70]). Periodic boundary conditions are applied to the simulation box, and placed in the center of the simulation box is a nanoparticle with an effective diameter 10 times the size of an individual monomer. Two monomer types are considered, A and B, differing only in that B monomers adsorb more strongly to the nanoparticle than A monomers.

The reduced units of mass, length and energy are m, σ, and ε respectively, which are defined based on the length scale and strength of the interaction between nonbonded monomers. As a result, the reduced unit of time is defined as $\tau = \sigma(m/\varepsilon)^{1/2}$. All monomers have a mass of $1.0m$, while the nanoparticle has a mass of $1000m$. The mapping of ε, σ, and m to real experimental units depends on the system being modeled, the temperature considered, and the degree of coarse-graining. Mapping τ to real time units in coarse-grained systems, however, is more complex since coarse-graining removes degrees of freedom and shortens timescales relative to atomistic simulations or experimental systems.[71,72] As an example, if the beads in our system were considered to represent approximately the mass and length scales of Kuhn segments of polybutadiene, and if the temperature modeled was considered to be close to room temperature, then ε, σ, m would take on values of approximately 2.5 kJ/mol, 0.99 nm, and 113 g/mol, respectively.[73] Using the most straightforward mapping (simply applying the equation $\tau = \sigma(m/\varepsilon)^{1/2}$) τ would be approximately 2×10^{-10} seconds. Since this mapping does not consider the lost degrees of freedom, the result is effectively a lower bound on τ. However, this example is only provided for reference; since the goal in this work is only to understand underlying physical mechanisms, this work will proceed using only reduced units.

Monomers are bonded using the Finitely Extensible Nonlinear Elastic (FENE) potential, defined as:

$$U_{\text{FENE}} = \begin{cases} -\frac{1}{2}kR_0{}^2 \ln\left[1 - \left(\frac{r}{R_0}\right)^2\right] & r \leq R_0 \\ 0 & r > R_0 \end{cases} \quad (1)$$

where r is the distance between the monomers, R_0 is the bond cutoff distance, (1.5σ), and k is a constant that sets the energy of the bond, for which a standard value of $k = 30\varepsilon/\sigma^2$ is used as suggested in literature to prevent chain crossing or scission.[69]

Unbonded monomer-monomer pairwise interactions follow a standard cut-off and shifted Lennard-Jones (LJ) potential, defined as:

$$U_{\text{LJ,ij}} = \begin{cases} 4\varepsilon_{\text{ij}}\left[\left(\frac{\sigma_{\text{ij}}}{r}\right)^{12} - \left(\frac{\sigma_{\text{ij}}}{r}\right)^{6}\right] + \delta_{\text{s}} & r \leq r_{\text{c}} \\ 0 & r > r_{\text{c}} \end{cases} \quad (2)$$

In this standard LJ potential, ε_{ij} is the interaction strength, σ_{ij} is the interaction length scale, and the subscripts i and j refer to the two monomer types. The cutoff distance, r_{c}, is set to $2^{\frac{1}{6}}\sigma_{\text{ij}}$ for bonded monomers and $2.5\sigma_{\text{ij}}$ for non-bonded monomers. δ_{s} is a vertical shift factor selected so that $U_{\text{LJ}}(r_c) = 0$. Because the monomers are idealized to differ only in interaction strength with the nanoparticle, monomer sizes and monomer-monomer interaction strengths do not depend on monomer type, so $\sigma_{\text{AA}} = \sigma_{\text{AB}} = \sigma_{\text{BB}} = 1.0\sigma$ and $\varepsilon_{\text{AA}} = \varepsilon_{\text{AB}} = \varepsilon_{\text{BB}} = 1.0\varepsilon$.

Unlike monomer-monomer interactions, monomer-nanoparticle interactions depend on monomer type. Here, a radially shifted LJ potential is utilized, which has been used to manage polymer-nanoparticle interactions in previous simulation studies of coarse-grained polymer nanocomposites.[8,13,17,74] This potential is defined as:

$$U_{\text{NM}} = \begin{cases} \infty & r - \Delta \leq 0 \\ 4\varepsilon_{\text{NM}} \left[\left(\frac{\sigma}{r-\Delta} \right)^{12} - \left(\frac{\sigma}{r-\Delta} \right)^{6} \right] + \delta & 0 < r - \Delta \leq r_{\text{c}} \\ 0 & r - \Delta > r_{\text{c}} \end{cases} \tag{3}$$

Here, σ_{NM} is the effective diameter of the nanoparticle, set to 10σ, and the shift factor $\Delta = (\sigma_{\text{NM}} - \sigma)/2 = 4.5\sigma$. The interaction strength, ε_{NM}, is a function of monomer type, M, with $\varepsilon_{\text{NA}} = 1$ and $\varepsilon_{\text{NB}} = 5$. Thus, A monomers have the same affinity for the nanoparticle as for other monomers, while B monomers adsorb strongly to the nanoparticle compared to other monomers. Note that the nanoparticle-A monomer interaction is effectively repulsive due to the nanoparticle being larger than the monomer, making A monomer that approaches the nanoparticle surface from the bulk lose multiple interactions with other monomers while gaining only one interaction with the nanoparticle.

This work studies the Pure B homopolymer system in addition to a number of AB copolymer systems. In the copolymer systems, each chain contains equal numbers of A and B monomers, but monomers are arranged in different configurations depending on the system. Specifically, this work focuses on a series of regular multiblock copolymer sequences with form $[\text{A}_{B_L}\text{B}_{B_L}]_y$, where $y = 100/(2B_L)$ and B_L is the length of each block. In this work, B_L is set to either 1, 2, or 25. These systems were chosen in order to approximately replicate previously synthesized experimental multiblock copolymer sequences with adjustable block length. The composition of these experimental polymer systems include poly(styrene-b-butadiene),[75,76] poly(lactide-b-butadiene)[77] and poly(styrene-b-methyl methacrylate).[78] In most current polymer-nanocomposite applicaitons, polymers are arranged randomly with a 50-50 split composition of the two monomers. However, systems containing chains with random sequence may not be optimally arranging the monomers in a way that the material exhibits the desired amount of hysteresis at given oscillatory strain frequen-

cies. Figure 2 shows a schematic of a few representative copolymer sequences from our study.

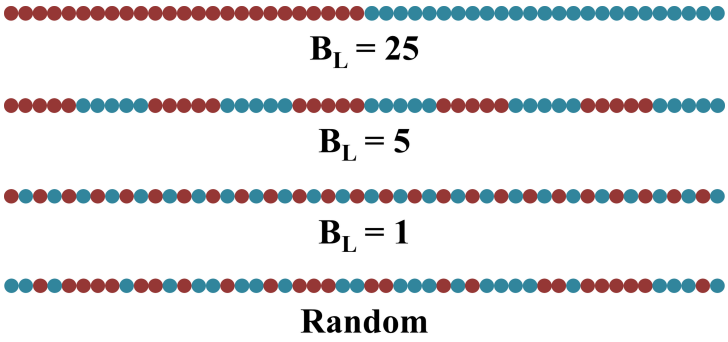

Figure 2: Schematic of different copolymer sequences used in this work. To simplify the schematic visually, each segment above shows one half of its corresponding N = 100 polymer chain.

Simulations were carried out using the open-source molecular dynamics (MD) package LAMMPS and applying the default equations of motion.[79] The initial positions of the polymer chains were generated as random walks where bonded monomers were 0.96σ apart. If monomer locations fell within the space of the nanoparticle, the monomer locations were rejected and regenerated. A soft pushoff phase before equilibration was used in order to correct monomer-monomer overlaps generated in the initial conditions. A timestep of $\delta t = 0.01$ was used throughout this study.

The first equilibration phase was conducted in an isobaric-isothermal (NPT) ensemble using a Nosé-Hoover thermostat (using damping parameters of 1.0) and barostat (with a damping parameter of 10.0) to hold the reduced temperature at 1.0 and the reduced pressure at 0. NPT equlibration ran for 200,000τ, or 20,000,000 timesteps. This time window was 10 times as long as the end-to-end vector autocorrelation function relaxation time in the bulk (approximately $1.9 \times 10^4\tau$), and during this time, the root mean squared displacement of all monomers reached 16.8σ, which is more than 3 times the average radius of gyration in the bulk (approximately 5.1σ).[67] Using these benchmarks, it is clear that the polymers had adequate time to span the simulation box and reach their preferred

conformations.

After NPT equilibration, a second equilibration phase was conducted in a microcannonical (NVE) ensemble by removing the thermostat and barostat and fixing the volume at the average volume of the last 1,000,000 timesteps of NPT equilibration. In each NVE equilibration phase, each side of the cubic simulation box was approximately 36σ in length. NVE equilibration ran for 50,000τ, or 5,000,000 timesteps, in order to ensure that the system had time to adjust to the new fixed volume. The size of the simulation box ensured that the radius of gyration was within 2% of its value in the bulk for polymers whose centers were 6σ from the box edge, and the A and B nanoparticle-monomer pair distribution functions were within 2% of 1.0 by 2σ from the box edge.

Once both equilibration phases were finished, monomer positions and Cartesian stress tensor values for each timestep were saved for analysis at every timestep in two trajectories which each ran for 100τ, or 10,000 timesteps, and whose initial configurations were separated by 50,000τ, or 5,000,000 timesteps. The time in between analysis windows was well past two relaxation times of the end-to-end vector autocorrelation function. At each timestep, Cartesian atomic stresses on each monomer are calculated according to:

$$\sigma_{i_{ab}} = -m_i v_{i_a} v_{i_b} - \frac{1}{2} \sum_{j \neq i} (r_{i_a} F_{ij_b} + r_{j_a} F_{ji_a}) \tag{4}$$

where a and b take on the values x, y, z to calculate each component of the symmetric Cartesian stress tensor, $\sigma_{i_{ab}}$ is atomic stress on bead i in direction ab, m_i is the mass of the monomer, v_i is the velocity of bead i, r_i is the position of bead i, and F_{ij} is the force that a particle j exerts on bead i. The force summation is performed over all particles in the system, which includes the nanoparticle. The calculation of each $\sigma_{i_{ab}}$ was carried out at each timestep of the trajectories. When $a = b$, the stress component is normal (which may be either tensile or compressive), and when $a \neq b$, the stress component is shear.

Once stress tensor and monomer position data in Cartesian coordinates was collected, the stress tensor data was then converted to spherical coordinates. Bead positions were

converted to spherical coordinates centered at the nanoparticle using basic trigonometry. The conversion of stress tensor components was calculated at each atom by calculating the following tensor dot product using both stress and position data:[80]

$$\begin{bmatrix} \sigma_{\rho\rho} & \sigma_{\rho\theta} & \sigma_{\rho\phi} \\ \sigma_{\theta\rho} & \sigma_{\theta\theta} & \sigma_{\theta\phi} \\ \sigma_{\phi\rho} & \sigma_{\phi\theta} & \sigma_{\phi\phi} \end{bmatrix} = \begin{bmatrix} sin\theta cos\phi & sin\theta sin\phi & cos\theta \\ cos\theta cos\phi & cos\theta sin\phi & -sin\theta \\ -sin\phi & cos\phi & 0 \end{bmatrix} \cdot \begin{bmatrix} \sigma_{xx} & \sigma_{xy} & \sigma_{xz} \\ \sigma_{yx} & \sigma_{yy} & \sigma_{yz} \\ \sigma_{zx} & \sigma_{zy} & \sigma_{zz} \end{bmatrix} \cdot \begin{bmatrix} sin\theta cos\phi & cos\theta cos\phi & -sin\phi \\ sin\theta sin\phi & cos\theta sin\phi & cos\phi \\ cos\theta & -sin\theta & 0 \end{bmatrix} \quad (5)$$

The same method as used in our previous work is used to estimate local dynamic modulus in this work.[42] Bulk dynamic modulus can be measured from an MD simulation using either non-equilibrium[71,81,82] or equilibrium[83–85] methods. In this work, the equilibrium method is used to estimate local dynamic modulus, where dynamic modulus can be measured from an MD simulation at equilibrium using the stress autocorrelation function (SACF):

$$G'(\omega) + iG''(\omega) = i\omega \frac{V}{k_{\mathrm{B}}T} \int_0^{+\infty} e^{-i\omega t} \langle \sigma(0)\sigma(t) \rangle \, \mathrm{d}t \quad (6)$$

where $\sigma(t)$ is the bulk stress at time t, $\langle \sigma(0)\sigma(t) \rangle$ is the SACF, V is the system volume, and $k_{\mathrm{B}}T$ is the thermal energy of the system. A Fourier transform is used to decompose the modulus into storage (G') and loss (G'') moduli, both of which are functions of the frequency of excitation, ω. As opposed to non-equilibrium methods of extracting bulk dynamic modulus, this method is more computationally efficient because moduli can be calculated for a range of frequencies from a single simulation. This technique has been used in previous works to compute dynamic moduli for a variety of systems.[83–89]

The works referenced above, however, measured the bulk SACF and calculated the bulk modulus as opposed to local dynamic modulus. In order to precisely measure local dynamic modulus, a locally defined measurement of the SACF that would vary as a function of position would be needed. However, SACF is a function of time, and atoms in the

system are not stationary in time, which makes defining and calculating a "local SACF" a non-trivial task. Instead, our method approximates the local SACF by dividing the system into concentric spherical shells centered on the nanoparticle and calculating $\langle\sigma(0)\sigma(t)\rangle_s$, an estimate of the average stress autocorrelation function of monomers in shell s. The result is then used with Equation 6 to estimate the dynamic storage and loss modulus for each individual shell.

To do this, at each shell and at each timestep t', the stress on each bead, i, that lies within a shell at t' is calculated according to Equation 4, and then a stress autocorrelation $\sigma_i(t')\sigma_i(t'+\Delta t)$ is calculated for each possible time window length Δt from 0.01τ to 8τ, or 1 to 800 timesteps. At each starting timestep t', this quantity is averaged over all monomers in each shell, yielding $[\sigma(t')\sigma(t'+\Delta t)]_s$, which is the average dissipation of stress for atoms that initially resided in shell s at time t'. $[\sigma(t')\sigma(t'+\Delta t)]_s$ is further averaged across all possible times, t', yielding $\langle\sigma(0)\sigma(\Delta t)\rangle_s$ for each shell. Therefore, our estimate of $\langle\sigma(t')\sigma(t'+\Delta t)\rangle_s$ is the average of $10,000-\Delta t/\delta t$ subwindows within each trajectory. These results are further averaged across each of the two trajectories, sampling the system at multiple different configurations that are separated by timescales longer than the end-to-end vector relaxation time.

Atoms assigned to each shell are not necessarily the same for each autocorrelation window starting timestep t', and atoms may also move outside their initial shell during the course of the autocorrelation time window. Because of this, our formulation of the SACF is only able to measure the average stress dissipation of atoms that initially reside in a given shell. To reduce the degree of approximation, the longest considered autocorrelation time window is $\Delta t = 8\tau$, or 800 timesteps. This time window was selected since the square root of the monomer mean squared displacement in the time window is less than 1.0, meaning that the average monomer does not move significantly more than a single shell width during a single autocorrelation time window. With these provisions in mind, this approximation of the local SACF will hereafter be referred to as the LSACF.

Becuase the system is isotropic, geometrically similar tensile components of the LSACF stress tensor are virtually equivalent and can be averaged into a stress paramter to improve statistics. Two shear stress parameters were collected at each atom i, σ_{i_ρ} to represent dynamic radial shear stresses and σ_{i_θ} to represent dynamic tangential shear stresses. σ_{i_ρ} was calculated by taking the average of the four radial shear components of the spherical stress tensor: $\sigma_{\theta\rho}$, $\sigma_{\phi\rho}$, $\sigma_{\rho\theta}$, and $\sigma_{\rho\phi}$. σ_{i_θ} was calculated by taking the average of the two tangential shear components of the spherical stress tensor: $\sigma_{\theta\phi}$ and $\sigma_{\phi\theta}$.

After this averaging, however, the results of the LSACF are quite noisy. To reduce the level of noise in the data, a running average filter is applied, similar to the one used by Sen *et al.*,[83] such that the final LSACF data at each time t is an average of all raw LSACF data points from $0.8\Delta t$ to $1.2\Delta t$. This filter uses a wider time window than in the work by Sen and colleagues since our system is divided into shells, meaning that fewer atoms are present in each ensemble. The effect from the filter on the magnitude of the LSACF results is small, and a comparison between results gathered with and without the filter can be obtained in the Supporting Information of our previous work.[42]

A final remaining challenge of this analysis method is that the autocorrelation data is truncated at 8τ, which results in a discontinuity after the time window of the Fourier Transform. The calculated storage and loss moduli exhibit substantial oscillations in the frequency domain due to this discontinuity. To minimize additional noise from this effect, the raw LSACF data is artificially extended after time filtering and prior to applying the Fourier transform by performing a power law fit on the existing data above 1τ and then extrapolating the data out to 1000τ. This data extension nearly eliminates oscillations in the dynamic modulus, yet leaving the overall magnitude mostly unchanged. The Supporting Information of our previous work additionally contains a comparison of dynamic modulus data calculated with and without the raw LSACF data extension.[42]

Results

In this work, each system is divided into concentric shells centered around the nanoparticle with a width of 0.5σ. Using the procedures detailed above, estimates of storage and loss modulus at each shell were obtained across the range of 800 frequencies. Bulk storage and loss modulus were collected using the typical methods using the bulk stress autocorrelation data with Equation 6. At each shell, radial shear and tangential shear moduli are calculated.

Using local estimates of storage modulus, G', and loss modulus, G'', an estimate of complex modulus is calculated using $|G^*| = \sqrt{G'^2 + G''^2}$ at each frequency, which gives the ratio of the amplitude of an input stress and the amplitude of the resulting strain. $tan(\delta)$ is additionally calculated, where δ is the phase lag angle of the shift between the input stress and resulting strain. $tan(\delta)$ can also be calculated as the ratio of loss modulus and storage modulus ($tan(\delta) = G''/G'$). $tan(\delta)$ is a useful metric in quantifying hysteresis in a material as it is a ratio of energy lost in the material to the energy returned by the material. Together, $|G^*|$ and $tan(\delta)$ completely characterize the behavior of a given material under a cyclical stress, and information about G' and G'' are encoded inside these two parameters.

The range of frequencies accessible for analysis are physically limited by the time intervals at which data is collected. At the low end, frequencies are bounded by the reciprocal of a period length equal to the longest correlation window. The reciprocal of a period length equal to the length of two timesteps (0.02τ) bounds the frequencies at the high end. Despite that the LSACF was artificially extended for smoothness of the data, the raw data sets are only 8τ in length, making the theoretical lower bound of analysis at $2\pi/8$ rad/τ. For visual clarity in figures presented in this work, analysis is truncated to 1 rad/τ, which is close to yet within the lower bound. The theoretical upper bound of analysis based on how the data was collected in this work is 300 rad/τ. However, analysis is only conducted up to 20 rad/τ in this work due to FENE bond vibrations becoming dominant in the results (as the natural bond vibration frequency was set to 30 rad/τ). This phenomenon has been

documented by other researchers.[83]

$tan(\delta)$ and $|G^*|$ results for multiple shells around the nanoparticle in the pure B homopolymer system are presented in Figure 3 and compared to the bulk.Complex modulus in both the radial shear and tangential shear geometries generally increases with respect to frequency and proximity to the nanoparticle. The ratio of complex modulus in the closest shell to the complex modulus in the bulk is around 8.0, a pattern that is also found when analysis is carried out in Cartesian coordinates.[42] Tangential complex modulus is generally slightly larger than radial complex modulus by a ratio of approximately 2.0 (although this ratio decreases in shells that are closer to the nanoparticle). Ratio between the moduli of two given shells, or mechanical reinforcement, is relatively independent of frequency. These patterns additionally appear in all other systems presented in this work.

Similarly to the results presented in the analysis in Cartesian coordinates, $tan(\delta)$ exhibits a symmetrical peak at around 9 rad$/\tau$ for all shells. The magnitude of this peak increases with proximity to the nanoparticle, and reaches the same magnitudes in the radial and tangential shear directions. This peak is more closely correlated to a valley in the storage modulus than to a peak in loss modulus. The frequency that the peak occurs at is notably close to the reciprocal of the average time that is required for an adsorbed monomer (in the shell residing between 5.5 and 6.0σ) to move 1σ, the distance between peaks in the monomer-nanoparticle pair distribution.[67] This suggests that the peak in $tan(\delta)$ is a result of the adsorption-desoprtion process that monomers undergo when moving at the surface of the nanoparticle. This hypothesis is further exemplified in our analysis in Cartesian coordinates, as the peak in hysteresis does not occur in the pure A homopolymer system where the monomer-nanoparticle interaciton potential was set to be the same as that of other monomers.

Now considering copolymer systems, the $tan(\delta)$ and $|G^*|$ results for the $B_{\mathrm{L}} = 1$ system are presented in Figure 4. Because of the close proximity of monomer blocks to each other due to the short block length, there are more A monomers at the surface of the

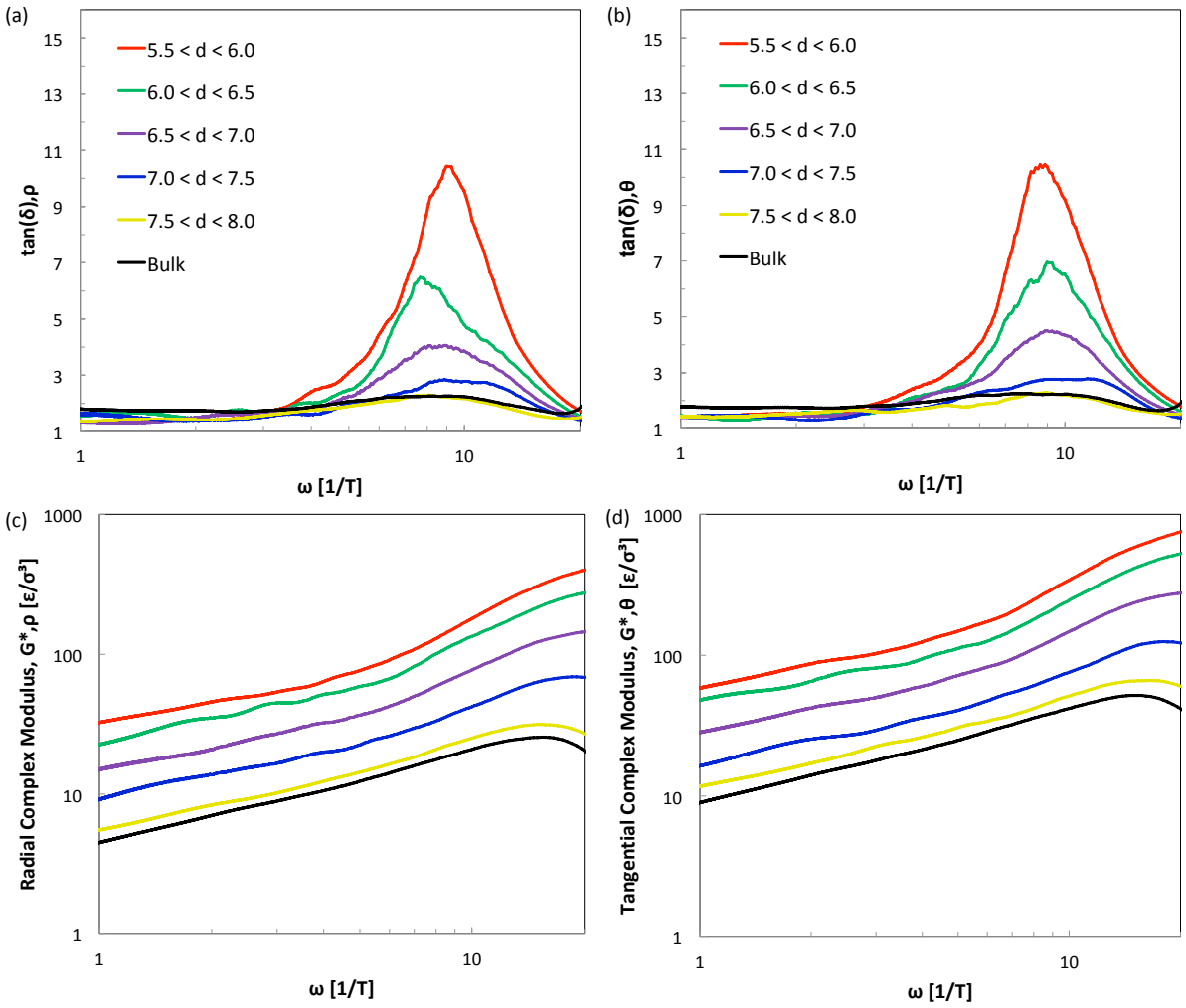

Figure 3: Radial shear hysteresis (a), tangential shear hysteresis (b), radial complex modulus (c), and tangential complex modulus (d) of the Pure B homopolymer system as a function of distance from the nanoparticle center, d. Shells are bounded by distance from the nanoparticle center as labeled, and monomers are assigned to shells as described in the text.

nanoparticle than in any other system, which makes for unusual patterns in the complex modulus and $tan(\delta)$ results. Notably different from the same analysis done in Cartesian coordinates, $|G^*|$ does not monotonically increase with proximity to the nanoparticle, as the second closest shell ($6.0 < d < 6.5$) has a higher complex modulus in the radial shear direction, while $|G^*|$ increases monotonically in the tangential shear direction. Other than this exception, the complex modulus results for this system (and all others presented in this work) have similar magnitudes and ratios between complex modulus in the closest shell and in the bulk to those found in the pure B homopolymer system.

The differences from the Cartesian analysis are more pronounced in the $tan(\delta)$ results, where both the second and third closest shells exhibit higher peak hysteresis than the closest shell. The hysteresis peaks occur at the same frequency and have the same width as the homopolymer system, but generally have a lower magnitude than in the homopolymer system (with the exception of the radial shear results for the third closest shell). Additionally, the tangential shear hysteresis at each shell has a lower magnitude than in the radial shear direction. These results suggest that in short block length copolymer nanocomposite materials undergoing oscillatory stress, most of the energy loss occurs in the radial direction for the monomers close to the nanoparticle.

The next system considered for spherical analysis of dynamic moduli was the $B_{\mathrm{L}} = 2$ copolymer system, which behaves differently from the $B_{\mathrm{L}} = 1$ despite being a small change in copolymer sequence block length. Complex modulus and $tan(\delta)$ results are presented for this system in Figure 5. Complex modulus yields mostly similar results to both the pure B homopolymer and $B_{\mathrm{L}} = 1$ systems, however reveals considerably different results in the data for $tan(\delta)$.

Unlike the $B_{\mathrm{L}} = 1$ copolymer system, radial shear and tangential shear hysteresis peaks for the closest shell to the nanoparticle have the same magnitude. This trend is present for all other shells except for the second closest shell ($6.0 < d < 6.5$), where the peak in $tan(\delta)$ in the radial shear direction is 2.5 times larger than the corresponding peak in the tan-

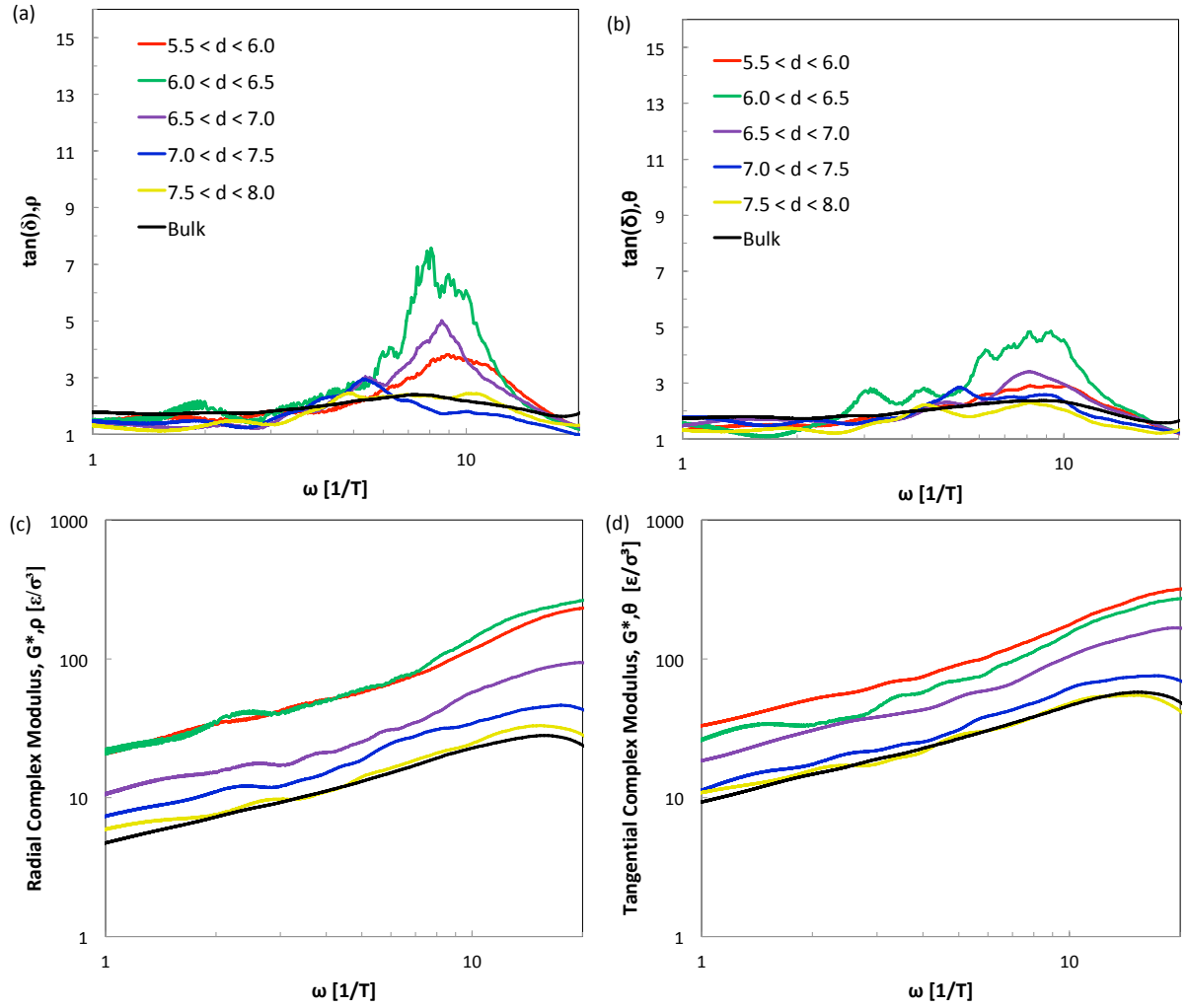

Figure 4: Radial shear hysteresis (a), tangential shear hysteresis (b), radial complex modulus (c), and tangential complex modulus (d) of the $B_L = 1$ copolymer system as a function of distance from the nanoparticle center, d. Shells are bounded by distance from the nanoparticle center as labeled, and monomers are assigned to shells as described in the text.

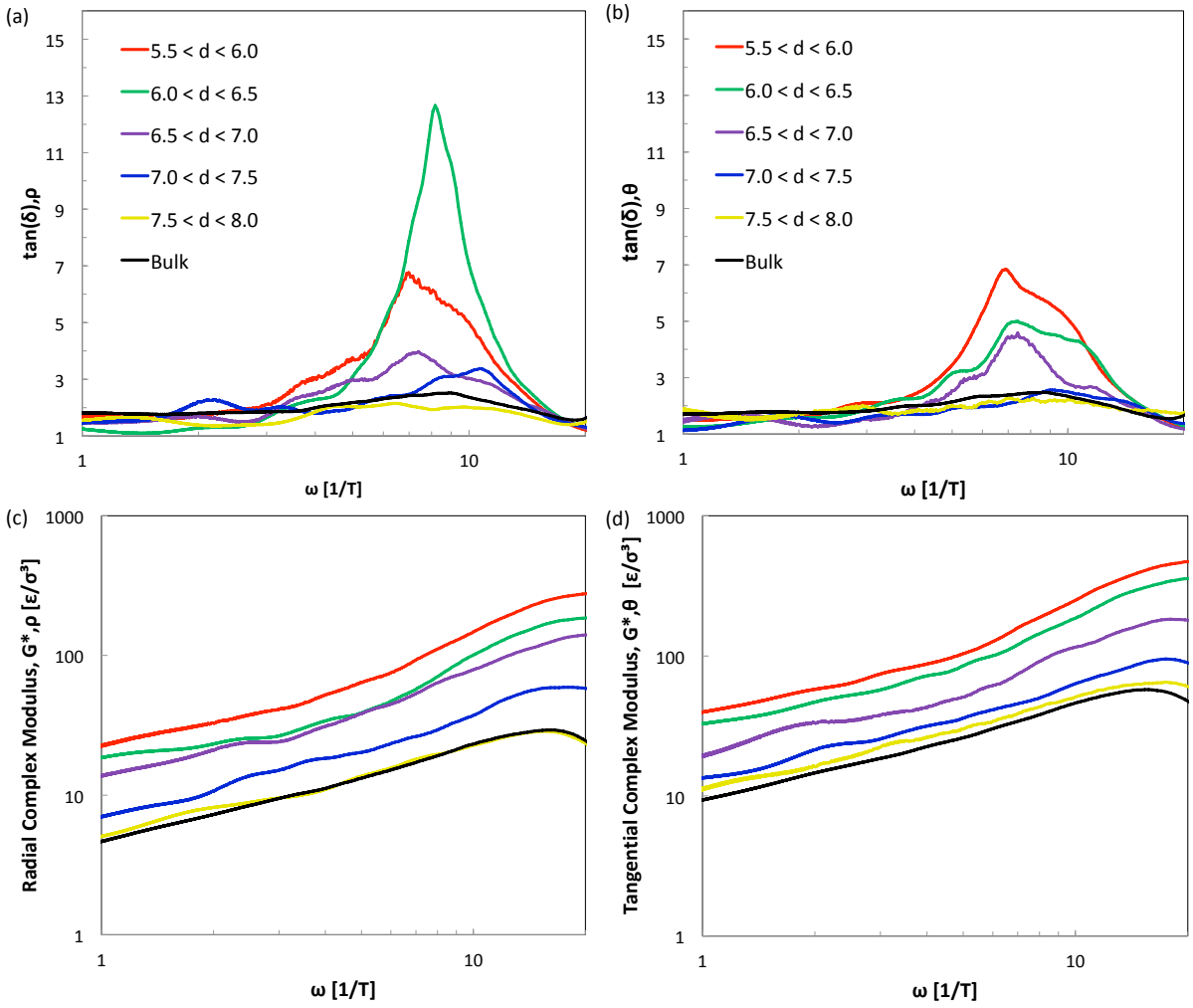

Figure 5: Radial shear hysteresis (a), tangential shear hysteresis (b), radial complex modulus (c), and tangential complex modulus (d) of the $B_L = 2$ copolymer system as a function of distance from the nanoparticle center, d. Shells are bounded by distance from the nanoparticle center as labeled, and monomers are assigned to shells as described in the text.

gential shear direction. This means that hysteresis in this system increases monotonically with proximity to the nanoparticle for the tangential shear direction, but not in the radial shear direction. The $tan(\delta)$ peak in the radial shear direction for the second shell is notably larger than for any system presented in this work, for both the radial and tangential shear directions. This phenomenon is likely due to the fact that the addition of a second B monomer in the blocks near the nanoparticle reduces the likelihood that A monomers would reside at the surface of the nanoparticle. However, because the A monomers are bonded so closely to the B monomers at the nanoparticle surface, it is likely that the effectively repellent A monomers "lock in place" in the space of the second closest shell to the nanoparticle when exposed to an oscillatory stress.

The last system analyzed in this work is the $B_{\mathrm{L}} = 25$ copolymer system, which has a significantly longer block length. The complex modulus and hysteresis results for this system are presented in Figure 6. This system has similar complex modulus results to the pure B homopolymer system and $B_{\mathrm{L}} = 2$ copolymer systems.

Both radial shear and tangential shear $tan(\delta)$ grow monotonically with proximity to the nanoparticle, a trend that does not occur in the other copolymer systems. The magnitudes of each of the peaks in $tan(\delta)$ are the same as the pure B homopolymer system except for the closest shell to the nanoparticle. For the closest shell, the radial shear $tan(\delta)$ peak is about 1.5 times larger than the tangential shear $tan(\delta)$ peak. The magnitude of the radial shear $tan(\delta)$ peak for the closest shell of the $B_{\mathrm{L}} = 25$ copolymer system is between that of the closest shell of the pure B homopolymer system and the $tan(\delta)$ peak that occurs for the second closest shell of the $B_{\mathrm{L}} = 2$ copolymer system. The magnitude of the hysteresis peak in the tangential shear direction, however, is almost the same for both the closest and second closest shells to the nanoparticle.

Taking into consideration the results from all systems presented in this work, it is clear that the hysteresis in the radial shear and tangential shear directions behave differently at close distances to the nanoparticle. The radial shear hysteresis is generally the larger of the

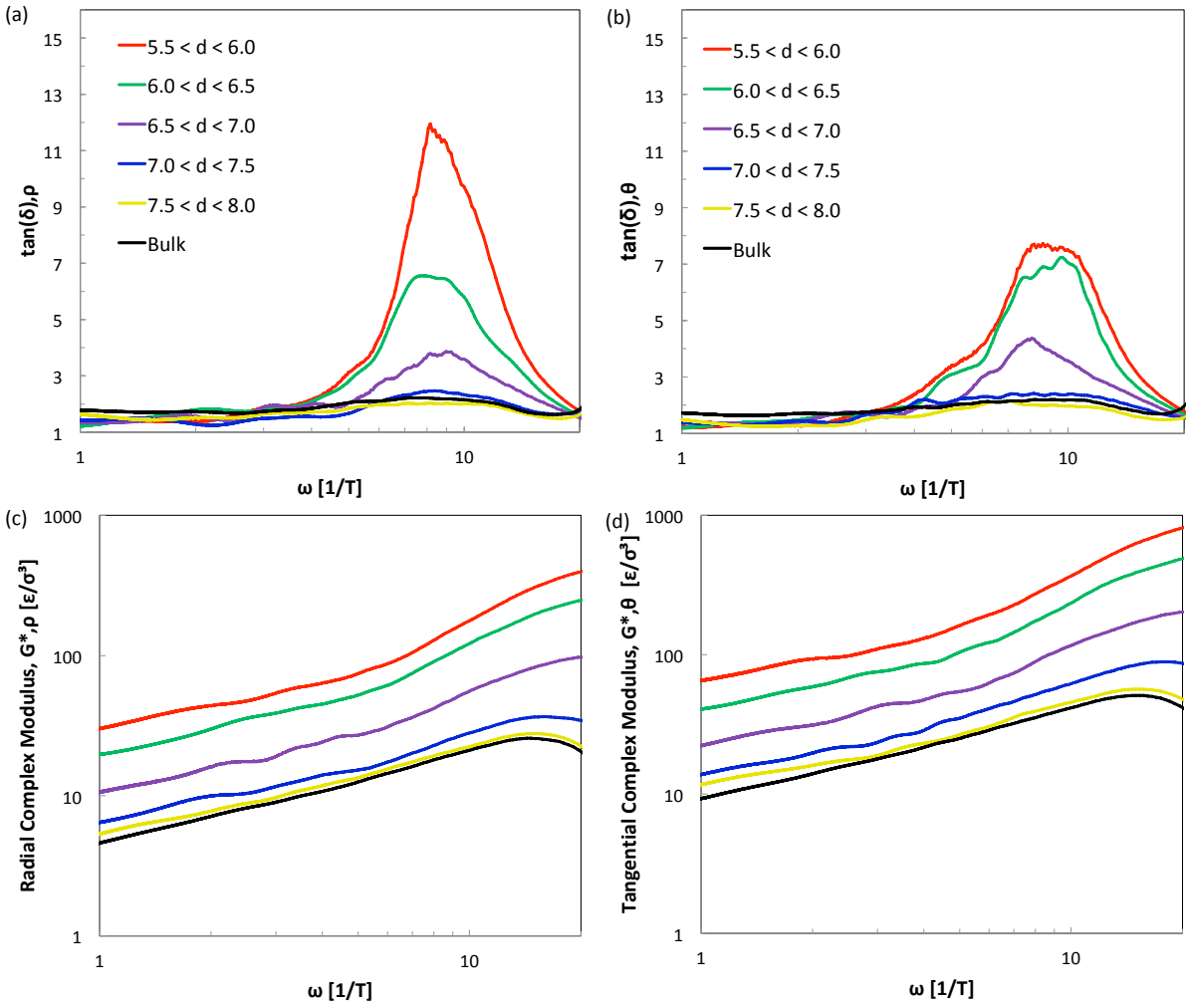

Figure 6: Radial shear hysteresis (a), tangential shear hysteresis (b), radial complex modulus (c), and tangential complex modulus (d) of the $B_L = 25$ copolymer system as a function of distance from the nanoparticle center, d. Shells are bounded by distance from the nanoparticle center as labeled, and monomers are assigned to shells as described in the text.

two hysteresis parameters, due to the presence of the nanoparticle. Even small changes in the block length of the copolymer system yielded significantly different results. These findings suggest that the peak in hysteresis is related to the adsorption-desorption process of monomers at the nanoparticle surface, a process that involves the radial movement of monomers. If this hypothesis is proven to be correct, this could allow material designers to focus their attention on adsorption-desoprtion parameters in order to tune material behavior.

Conclusions

Conducting a localized analysis of dynamic moduli using the stress autocorrelation function and converting the results to spherical coordinates surrounding a nanoparticle, estimations of local complex modulus and hysteresis were gathered for a variety of polymer-nanocomposite systems. Splitting the results into radial shear and tangential shear parameters provides a deeper understanding of the underlying trends observed in Cartesian coordinates. The results point to radial shear moduli being dominant for monomers that are close to the nanoparticle surface. The results from this paper further demonstrate how tuning the copolymer sequence can dramatically alter the extent by which radial shear moduli alter the behavior of the material near the nanoparticle surface.

The results in this paper elaborate upon the observed behavior found in the previous analysis in Cartesian coordinates, suggesting potential underlying driving forces that explain the trends. If the hypothesis that the peak in hysteresis is a result of adsorption-desoprtion processes, material designers can focus on gathering data about polymer-filler adsorption to predict at what frequency a $tan(\delta)$ peak would occur in material applications. Material designs that optimize hysteresis across a wide range of excitation frequencies could minimize the trade off between traction and rolling resistance (fuel efficiency), as an example.

In future works, analysis can be performed on polymer-nanocomposite systems where polymers are crosslinked to see if changes in the macro-structure of the polymer chains has an effect on the peak in hysteresis. Analysis of more copolymer configurations (such as tapered or inverse-tapered copolymer sequences) may also reveal additional effects of tuning copolymer sequence. Finally, running the same analysis on systems where nanoparticles have a different radius of curvature may have an impact on local behavior as well, as suggested in previous works.[63] Overall, the goal is to develop a complete understanding of the underlying mechanisms that govern the properties of polymer-nanoparticle interphases, which provides a understanding on how to tune copolymer sequence to produce desired mechanical properties.

Acknowledgement

This material is based upon work supported by the National Science Foundation under Grant No. 1454343. This material was also partially supported by an Exploratory Materials Research Grant from the OSU Materials Research Seed Grant Program of the Institute for Materials Research (IMR) at The Ohio State University. The author of this work also acknowledges the Ohio Supercomputing Center for providing an allocation of computing time. The author additionally thanks Tarik Akyuz for developing portions of the analysis code. The Cooper Tire and Rubber Company also funded a portion of this project, and this work was improved by helpful discussions with several Cooper Tire researchers, especially Dr. Patrick Majors.

References

(1) Ge, T.; Kalathi, J. T.; Halverson, J. D.; Grest, G. S.; Rubinstein, M. Nanoparticle Motion in Entangled Melts of Linear and Nonconcatenated Ring Polymers. *Macromolecules* **2017**, *50*, 1749–1754, DOI: 10.1021/acs.macromol.6b02632.

(2) Griffin, P. J.; Bocharova, V.; Middleton, L. R.; Composto, R. J.; Clarke, N.; Schweizer, K. S.; Winey, K. I. Influence of the Bound Polymer Layer on Nanoparticle Diffusion in Polymer Melts. *ACS Macro Letters* **2016**, *5*, 1141–1145, DOI: 10.1021/acsmacrolett.6b00649.

(3) Kumar, S. K.; Krishnamoorti, R. Nanocomposites: Structure, Phase Behavior, and Properties. *Annual Review of Chemical and Biomolecular Engineering* **2010**, *1*, 37–58, DOI: 10.1146/annurev-chembioeng-073009-100856.

(4) Sarvestani, A. S.; Jabbari, E. Modeling the Viscoelastic Response of Suspension of Particles in Polymer Solution: The Effect of Polymer-Particle Interactions. *Macromolecular Theory and Simulations* **2007**, *16*, 378–385, DOI: 10.1002/mats.200700009.

(5) Chao, H.; Riggleman, R. A. Effect of particle size and grafting density on the mechanical properties of polymer nanocomposites. *Polymer* **2013**, *54*, 5222–5229, DOI: 10.1016/j.polymer.2013.07.018.

(6) Picu, R. C.; Rakshit, A. Dynamics of free chains in polymer nanocomposites. *The Journal of Chemical Physics* **2007**, *126*, 144909, DOI: 10.1063/1.2719196.

(7) Starr, F. W.; Douglas, J. F.; Glotzer, S. C. Origin of particle clustering in a simulated polymer nanocomposite and its impact on rheology. *Journal of Chemical Physics* **2003**, *119*, 1777.

(8) Li, Y.; Kröger, M.; Liu, W. K. Nanoparticle Effect on the Dynamics of Polymer Chains

and Their Entanglement Network. *Physical Review Letters* **2012**, *109*, 118001, DOI: 10.1103/PhysRevLett.109.118001.

(9) Li, Y.; Kröger, M.; Liu, W. K. Nanoparticle Geometrical Effect on Structure, Dynamics and Anisotropic Viscosity of Polyethylene Nanocomposites. *Macromolecules* **2012**, *45*, 2099–2112, DOI: 10.1021/ma202289a.

(10) Starr, F. W.; Douglas, J. F. Modifying Fragility and Collective Motion in Polymer Melts with Nanoparticles. *Physical Review Letters* **2011**, *106*, 115702, DOI: 10.1103/PhysRevLett.106.115702.

(11) Kalathi, J. T.; Grest, G. S.; Kumar, S. K. Universal Viscosity Behavior of Polymer Nanocomposites. *Physical Review Letters* **2012**, *109*, 198301, DOI: 10.1103/PhysRevLett.109.198301.

(12) Song, Y.; Luo, M.; Dai, L. L. Understanding Nanoparticle Diffusion and Exploring Interfacial Nanorheology using Molecular Dynamics Simulations. *Langmuir* **2010**, *26*, 5–9, DOI: 10.1021/la901902t.

(13) Sorichetti, V.; Hugouvieux, V.; Kob, W. Structure and Dynamics of a Polymer–Nanoparticle Composite: Effect of Nanoparticle Size and Volume Fraction. *Macromolecules* **2018**, *51*, 5375–5391, DOI: 10.1021/acs.macromol.8b00840.

(14) Ghanbari, A.; Ndoro, T. V. M.; Leroy, F.; Rahimi, M.; Böhm, M. C.; Müller-Plathe, F. Interphase Structure in Silica–Polystyrene Nanocomposites: A Coarse-Grained Molecular Dynamics Study. *Macromolecules* **2012**, *45*, 572–584, DOI: 10.1021/ma202044e.

(15) Pandey, Y. N.; Papakonstantopoulos, G. J.; Doxastakis, M. Polymer/Nanoparticle Interactions: Bridging the Gap. *Macromolecules* **2013**, *46*, 5097–5106, DOI: 10.1021/ma400444w.

(16) Maurel, G.; Goujon, F.; Schnell, B.; Malfreyt, P. Multiscale Modeling of the Polymer–Silica Surface Interaction: From Atomistic to Mesoscopic Simulations. *The Journal of Physical Chemistry C* **2015**, *119*, 4817–4826, DOI: 10.1021/jp510979d.

(17) Padmanabhan, V.; Frischknecht, A. L.; Mackay, M. E. Effect of Chain Stiffness on Nanoparticle Segregation in Polymer/Nanoparticle Blends Near a Substrate. *Macromolecular Theory and Simulations* **2012**, *21*, 98–105, DOI: 10.1002/mats.201100048.

(18) Chen, T.; Qian, H.-J.; Zhu, Y.-L.; Lu, Z.-Y. Structure and Dynamics Properties at Interphase Region in the Composite of Polystyrene and Cross-Linked Polystyrene Soft Nanoparticle. *Macromolecules* **2015**, *48*, 2751–2760, DOI: 10.1021/ma502383n.

(19) Starr, F. W.; Schrøder, T. B.; Glotzer, S. C. Molecular Dynamics Simulation of a Polymer Melt with a Nanoscopic Particle. *Macromolecules* **2002**, *35*, 4481–4492, DOI: 10.1021/ma010626p.

(20) Dionne, P. J.; Picu, C. R.; Ozisik, R. Adsorption and Desorption Dynamics of Linear Polymer Chains to Spherical Nanoparticles: A Monte Carlo Investigation. *Macromolecules* **2006**, *39*, 3089–3092, DOI: 10.1021/ma0527754.

(21) Johnston, K.; Harmandaris, V. Hierarchical simulations of hybrid polymer–solid materials. *Soft Matter* **2013**, *9*, 6696–6710, DOI: 10.1039/C3SM50330E.

(22) Johnston, K.; Harmandaris, V. Hierarchical Multiscale Modeling of Polymer–Solid Interfaces: Atomistic to Coarse-Grained Description and Structural and Conformational Properties of Polystyrene–Gold Systems. *Macromolecules* **2013**, *46*, 5741–5750, DOI: 10.1021/ma400357r.

(23) Munaò, G.; Pizzirusso, A.; Kalogirou, A.; De Nicola, A.; Kawakatsu, T.; Müller-Plathe, F.; Milano, G. Molecular Structure and Multi-Body Potential of Mean Force in Silica-Polystyrene Nanocomposites. *arXiv:1809.06170 [cond-mat, physics:physics]* **2018**, arXiv: 1809.06170.

(24) Ndoro, T. V. M.; Voyiatzis, E.; Ghanbari, A.; Theodorou, D. N.; Böhm, M. C.; Müller-Plathe, F. Interface of Grafted and Ungrafted Silica Nanoparticles with a Polystyrene Matrix: Atomistic Molecular Dynamics Simulations. *Macromolecules* **2011**, *44*, 2316–2327, DOI: 10.1021/ma102833u.

(25) Ndoro, T. V. M.; Böhm, M. C.; Müller-Plathe, F. Interface and Interphase Dynamics of Polystyrene Chains near Grafted and Ungrafted Silica Nanoparticles. *Macromolecules* **2012**, *45*, 171–179, DOI: 10.1021/ma2020613.

(26) Ghanbari, A.; Rahimi, M.; Dehghany, J. Influence of Surface Grafted Polymers on the Polymer Dynamics in a Silica–Polystyrene Nanocomposite: A Coarse-Grained Molecular Dynamics Investigation. *The Journal of Physical Chemistry C* **2013**, *117*, 25069–25076, DOI: 10.1021/jp407109r.

(27) Voyiatzis, E.; Rahimi, M.; Müller-Plathe, F.; Böhm, M. C. How Thick Is the Polymer Interphase in Nanocomposites? Probing It by Local Stress Anisotropy and Gas Solubility. *Macromolecules* **2014**, *47*, 7878–7889, DOI: 10.1021/ma500556q.

(28) Jouault, N.; Crawford, M. K.; Chi, C.; Smalley, R. J.; Wood, B.; Jestin, J.; Melnichenko, Y. B.; He, L.; Guise, W. E.; Kumar, S. K. Polymer Chain Behavior in Polymer Nanocomposites with Attractive Interactions. *ACS Macro Letters* **2016**, *5*, 523–527, DOI: 10.1021/acsmacrolett.6b00164.

(29) Cheng, S.; Carroll, B.; Bocharova, V.; Carrillo, J.-M.; Sumpter, B. G.; Sokolov, A. P. Focus: Structure and dynamics of the interfacial layer in polymer nanocomposites with attractive interactions. *The Journal of Chemical Physics* **2017**, *146*, 203201, DOI: 10.1063/1.4978504.

(30) Robertson, C. G.; Lin, C. J.; Rackaitis, M.; Roland, C. M. Influence of Particle Size and Polymer-Filler Coupling on Viscoelastic Glass Transition of Particle-Reinforced Polymers. *Macromolecules* **2008**, *41*, 2727–2731, DOI: 10.1021/ma7022364.

(31) Fröhlich, J.; Niedermeier, W.; Luginsland, H.-D. The effect of filler–filler and filler–elastomer interaction on rubber reinforcement. *Composites Part A: Applied Science and Manufacturing* **2005**, *36*, 449–460, DOI: 10.1016/j.compositesa.2004.10.004.

(32) Kaewsakul, W.; Sahakaro, K.; Dierkes, W. K.; Noordermeer, J. W. Mechanistic aspects of silane coupling agents with different functionalities on reinforcement of silica-filled natural rubber compounds. *Polymer Engineering and Science* **2015**, *55*, 836+, 836.

(33) Fu, S.-Y.; Feng, X.-Q.; Lauke, B.; Mai, Y.-W. Effects of particle size, particle/matrix interface adhesion and particle loading on mechanical properties of particulate–polymer composites. *Composites Part B: Engineering* **2008**, *39*, 933–961, DOI: 10.1016/j.compositesb.2008.01.002.

(34) Ganesan, V.; Pryamitsyn, V.; Surve, M.; Narayanan, B. Noncontinuum effects in nanoparticle dynamics in polymers. *Journal of Chemical Physics* **2006**, *124*, 221102, DOI: 10.1063/1.2209241.

(35) Wang, M.; Hill, R. J. Anomalous bulk viscosity of polymer-nanocomposite melts. *Soft Matter* **2009**, *5*, 3940, DOI: 10.1039/b905686f.

(36) Brinke, J. W. t.; Debnath, S. C.; Reuvekamp, L. A. E. M.; Noordermeer, J. W. M. Mechanistic aspects of the role of coupling agents in silica–rubber composites. *Composites Science and Technology* **2003**, *63*, 1165–1174, DOI: 10.1016/S0266-3538(03)00077-0.

(37) Cheng, X.; Putz, K. W.; Wood, C. D.; Brinson, L. C. Characterization of Local Elastic Modulus in Confined Polymer Films via AFM Indentation. *Macromolecular Rapid Communications* **2015**, *36*, 391–397, DOI: 10.1002/marc.201400487.

(38) Cech, V.; Palesch, E.; Lukes, J. The glass fiber–polymer matrix interface/interphase characterized by nanoscale imaging techniques. *Composites Science and Technology* **2013**, *83*, 22–26, DOI: 10.1016/j.compscitech.2013.04.014.

(39) Young, T. J.; Monclus, M.; Broughton, W. R.; Ogin, S. L.; Smith, P. A. Observations on interphase characterisation in polymer composites by nanoscale indentation and use of AFM cantilever torsion to identify measurement artefacts. *Plastics, Rubber and Composites* **2012**, *41*, 240–246.

(40) Born, M.; Huang, K. *Dynamical Theory of Crystal Lattices*; Clarendon Press: Oxford : New York, 1998.

(41) Lutsko, J. F. Stress and elastic constants in anisotropic solids: Molecular dynamics techniques. *Journal of Applied Physics* **1988**, *64*, 1152–1154, DOI: 10.1063/1.341877.

(42) Trazkovich, A. J.; Wendt, M. F.; Hall, L. M. Effect of Copolymer Sequence on Local Viscoelastic Properties near a Nanoparticle. *Macromolecules* **2019**,

(43) Grosch, K. A. The Rolling Resistance, Wear and Traction Properties of Tread Compounds. *Rubber Chemistry and Technology* **1996**, *69*, 495–568, OCLC: 205646894.

(44) Wrana, C.; Eisele, U.; Kelbch, S. Measurement and molecular modeling of rolling resistance in tire treads. *ResearchGate* **2000**, *53*, 126–128.

(45) Evans, M. S.; Rapra Technology Limited, *Tyre compounding for improved performance*; Rapra Technology: Shawbury, Shrewsbury, Shropshire, U.K., 2002; OCLC: 246660131.

(46) Le Gal, A.; Klüppel, M. Investigation and modelling of rubber stationary friction on rough surfaces. *Journal of Physics: Condensed Matter* **2008**, *20*, 015007, DOI: 10.1088/0953-8984/20/01/015007.

(47) Heinrich, G.; Klüppel, M. Rubber friction, tread deformation and tire traction. *Wear* **2008**, *265*, 1052–1060, DOI: 10.1016/j.wear.2008.02.016.

(48) Modica, K. J.; Martin, T. B.; Jayaraman, A. Effect of Polymer Architecture on the Structure and Interactions of Polymer Grafted Particles: Theory and Simulations. *Macromolecules* **2017**, *50*, 4854–4866, DOI: 10.1021/acs.macromol.7b00524.

(49) Estridge, C. E.; Jayaraman, A. Assembly of diblock copolymer functionalized spherical nanoparticles as a function of copolymer composition. *The Journal of Chemical Physics* **2014**, *140*, 144905, DOI: 10.1063/1.4870592.

(50) Jayaraman, A. Polymer grafted nanoparticles: Effect of chemical and physical heterogeneity in polymer grafts on particle assembly and dispersion. *Journal of Polymer Science Part B: Polymer Physics* **2013**, *51*, 524–534, DOI: 10.1002/polb.23260.

(51) Yang, S.; Liu, S.; Narayanan, S.; Zhang, C.; Akcora, P. Chemical heterogeneity in interfacial layers of polymer nanocomposites. *Soft Matter* **2018**, *14*, 4784–4791, DOI: 10.1039/C8SM00663F.

(52) Senses, E.; Isherwood, A.; Akcora, P. Reversible Thermal Stiffening in Polymer Nanocomposites. *ACS Applied Materials & Interfaces* **2015**, *7*, 14682–14689, DOI: 10.1021/acsami.5b02046.

(53) Senses, E.; Faraone, A.; Akcora, P. Microscopic Chain Motion in Polymer Nanocomposites with Dynamically Asymmetric Interphases | NIST. *Scientific Reports* **2016**, *6*.

(54) Raja, S. N.; Olson, A. C. K.; Limaye, A.; Thorkelsson, K.; Luong, A.; Lin, L.; Ritchie, R. O.; Xu, T.; Alivisatos, A. P. Influence of three-dimensional nanoparticle branching on the Young's modulus of nanocomposites: Effect of interface orientation. *Proceedings of the National Academy of Sciences of the United States of America* **2015**, *112*, 6533–6538, DOI: 10.1073/pnas.1421644112.

(55) Sarkar, B.; Alexandridis, P. Block copolymer–nanoparticle composites: Structure, functional properties, and processing. *Progress in Polymer Science* **2015**, *40*, 33–62, DOI: 10.1016/j.progpolymsci.2014.10.009.

(56) Zhang, Q.; Zhang, L.; Lin, J. Percolating Behavior of Nanoparticles in Block Copolymer Host: Hybrid Particle-Field Simulations. *The Journal of Physical Chemistry C* **2017**, *121*, 23705–23715, DOI: 10.1021/acs.jpcc.7b07337.

(57) Chen, P.; Yang, Y.; Dong, B.; Huang, Z.; Zhu, G.; Cao, Y.; Yan, L.-T. Polymerization-Induced Interfacial Self-Assembly of Janus Nanoparticles in Block Copolymers: Reaction-Mediated Entropy Effects, Diffusion Dynamics, and Tailorable Micromechanical Behaviors. *Macromolecules* **2017**, *50*, 2078–2091, DOI: 10.1021/acs.macromol.7b00012.

(58) Huang, Z.; Chen, P.; Yang, Y.; Yan, L.-T. Shearing Janus Nanoparticles Confined in Two-Dimensional Space: Reshaped Cluster Configurations and Defined Assembling Kinetics. *The Journal of Physical Chemistry Letters* **2016**, *7*, 1966–1971, DOI: 10.1021/acs.jpclett.6b00724.

(59) Liang, R.; Xu, J.; Li, W.; Liao, Y.; Wang, K.; You, J.; Zhu, J.; Jiang, W. Precise Localization of Inorganic Nanoparticles in Block Copolymer Micellar Aggregates: From Center to Interface. *Macromolecules* **2015**, *48*, 256–263, DOI: 10.1021/ma501835r.

(60) Dong, B.; Guo, R.; Yan, L.-T. Coassembly of Janus Nanoparticles in Asymmetric Diblock Copolymer Scaffolds: Unconventional Entropy Effect and Role of Interfacial Topology. *Macromolecules* **2014**, *47*, 4369–4379, DOI: 10.1021/ma500161j.

(61) Chen, H.; Ruckenstein, E. Micellar Structures in Nanoparticle-Multiblock Copolymer Complexes. *Langmuir* **2014**, *30*, 3723–3728, DOI: 10.1021/la500450b.

(62) Martin, T.; McKinney, C.; Jayaraman, A. Effect of blockiness in grafted monomer se-

quences on assembly of copolymer grafted nanoparticles : a Monte Carlo simulation study. *Soft Matter* **2013**, *9*, 155–169, DOI: 10.1039/C2SM26611C.

(63) Banerjee, D.; Schweizer, K. S. Controlling effective interactions and spatial dispersion of nanoparticles in multiblock copolymer melts. *Journal of Polymer Science Part B: Polymer Physics* **2015**, *53*, 1098–1111, DOI: 10.1002/polb.23752.

(64) Banerjee, D.; Dadmun, M.; Sumpter, B.; Schweizer, K. S. Theory of the Miscibility of Fullerenes in Random Copolymer Melts. *Macromolecules* **2013**, *46*, 8732–8743, DOI: 10.1021/ma4017604.

(65) Hall, L. M.; Schweizer, K. S. Impact of Monomer Sequence, Composition and Chemical Heterogeneity on Copolymer-Mediated Effective Interactions between Nanoparticles in Melts. *Macromolecules* **2011**, *44*, 3149–3160, DOI: 10.1021/ma200079z.

(66) Xu, Q.; Chen, L.; Yang, F.; Cao, H. Integral Equation Prediction of the Structure of Alternating Copolymer Nanocomposites near a Substrate. *Langmuir* **2018**, DOI: 10.1021/acs.langmuir.8b01882.

(67) Trazkovich, A. J.; Wendt, M. F.; Hall, L. M. Effect of copolymer sequence on structure and relaxation times near a nanoparticle surface. *Soft Matter* **2018**, *14*, 5913–5921, DOI: 10.1039/C8SM00976G.

(68) Kremer, K.; Grest, G. S. Dynamics of entangled linear polymer melts: A molecular-dynamics simulation. *The Journal of Chemical Physics* **1990**, *92*, 5057–5086, DOI: doi:10.1063/1.458541.

(69) Grest, G. S.; Lacasse, M.-D.; Kremer, K.; Gupta, A. M. Efficient continuum model for simulating polymer blends and copolymers. *The Journal of Chemical Physics* **1996**, *105*, 10583–10594, DOI: doi:10.1063/1.472978.

(70) Hoy, R. S.; Foteinopoulou, K.; Kröger, M. Topological analysis of polymeric melts: Chain-length effects and fast-converging estimators for entanglement length. *Physical Review E* **2009**, *80*, 031803, DOI: 10.1103/PhysRevE.80.031803.

(71) Sampath, J.; Hall, L. M. Impact of ionic aggregate structure on ionomer mechanical properties from coarse-grained molecular dynamics simulations. *The Journal of Chemical Physics* **2017**, *147*, 134901, DOI: 10.1063/1.4985904.

(72) Larson, R. G. Principles for coarse-graining polymer molecules in simulations of polymer fluid mechanics. *Molecular Physics* **2004**, *102*, 341–351, DOI: 10.1080/00268970310001640102.

(73) Rubinstein, M.; Colby, R. H. *Polymer Physics*, 1st ed.; Oxford University Press: Oxford ; New York, 2003.

(74) Liu, J.; Wu, Y.; Shen, J.; Gao, Y.; Zhang, L.; Cao, D. Polymer – nanoparticle interfacial behavior revisited: A molecular dynamics study. *Physical Chemistry Chemical Physics* **2011**, *13*, 13058–13069, DOI: 10.1039/C0CP02952A.

(75) Mastan, E.; He, J. Continuous Production of Multiblock Copolymers in a Loop Reactor: When Living Polymerization Meets Flow Chemistry. *Macromolecules* **2017**, *50*, 9173–9187, DOI: 10.1021/acs.macromol.7b01662.

(76) Lee, I.; Bates, F. S. Synthesis, Structure, and Properties of Alternating and Random Poly(styrene-b-butadiene) Multiblock Copolymers. *Macromolecules* **2013**, *46*, 4529–4539, DOI: 10.1021/ma400479b.

(77) Lee, I.; Panthani, T. R.; Bates, F. S. Sustainable Poly(lactide-b-butadiene) Multiblock Copolymers with Enhanced Mechanical Properties. *Macromolecules* **2013**, *46*, 7387–7398, DOI: 10.1021/ma401508b.

(78) Sugiyama, K.; Oie, T.; El-Magd, A. A.; Hirao, A. Synthesis of Well-Defined (AB)n Multiblock Copolymers Composed of Polystyrene and Poly(methyl methacrylate) Segments Using Specially Designed Living AB Diblock Copolymer Anion. *Macromolecules* **2010**, *43*, 1403–1410, DOI: 10.1021/ma902473t.

(79) Shinoda, W.; Shiga, M.; Mikami, M. Rapid estimation of elastic constants by molecular dynamics simulation under constant stress. *Phys. Rev. B Physical Review B* **2004**, *69*, OCLC: 4633043411.

(80) Continuum Mechanics - Polar Coordinates. Brown University, 2018; http://www.brown.edu/Departments/Engineering/Courses/En221/Notes/Polar_Coords/Polar_Coords.htm.

(81) Vladkov, M.; Barrat, J.-L. Linear and nonlinear viscoelasticity of a model polymer melt: Molecular Dynamics and Rouse Modes analysis. *arXiv:cond-mat/0507229* **2005**, arXiv: cond-mat/0507229.

(82) Ayton, G.; Smondyrev, A. M.; Bardenhagen, S. G.; McMurtry, P.; Voth, G. A. Calculating the bulk modulus for a lipid bilayer with nonequilibrium molecular dynamics simulation. *Biophysical Journal* **2002**, *82*, 1226–1238, DOI: 10.1016/S0006-3495(02)75479-9.

(83) Sen, S.; Kumar, S. K.; Keblinski, P. Viscoelastic Properties of Polymer Melts from Equilibrium Molecular Dynamics Simulations. *Macromolecules* **2005**, *38*, 650–653, DOI: 10.1021/ma0354871.

(84) Nevins, D.; Spera, F. J. Accurate computation of shear viscosity from equilibrium molecular dynamics simulations. *Molecular Simulation* **2007**, *33*, 1261–1266, DOI: 10.1080/08927020701675622.

(85) Wittmer, J. P.; Xu, H.; Benzerara, O.; Baschnagel, J. Fluctuation-dissipation relation between shear stress relaxation modulus and shear stress autocor-

relation function revisited. *Molecular Physics* **2015**, *113*, 2881–2893, DOI: 10.1080/00268976.2015.1023225, arXiv: 1508.03731.

(86) Vladkov, M.; Barrat, J.-L. Linear and Nonlinear Viscoelasticity of a Model Unentangled Polymer Melt: Molecular Dynamics and Rouse Modes Analysis. *Macromolecular Theory and Simulations* **2006**, *15*, 252–262, DOI: 10.1002/mats.200500079.

(87) Zhou, Q.; Larson, R. G. Direct Calculation of the Tube Potential Confining Entangled Polymers. *Macromolecules* **2006**, *39*, 6737–6743, DOI: 10.1021/ma060670a.

(88) Likhtman, A. E.; Sukumaran, S. K.; Ramirez, J. Linear Viscoelasticity from Molecular Dynamics Simulation of Entangled Polymers. *Macromolecules* **2007**, *40*, 6748–6757, DOI: 10.1021/ma070843b.

(89) Lee, W. B.; Kremer, K. Entangled Polymer Melts: Relation between Plateau Modulus and Stress Autocorrelation Function. *Macromolecules* **2009**, *42*, 6270–6276, DOI: 10.1021/ma9008498.